Modelling Crack Initiation in Bituminous Binders under a Rotational Shear Fatigue Load

Yangming Gao, PhD
Aston Institute of Materials Resear[1]ch
School of Engineering and Applied Science
Aston University, Birmingham, United Kingdom, B4 7ET
Email: gaoy14@aston.ac.uk

Linglin Li, PhD
Aston Institute of Materials Research
Aston University, Birmingham, United Kingdom, B4 7ET
Email: l.li28@aston.ac.uk

Yuqing Zhang, PhD
Aston Institute of Materials Research
School of Engineering and Applied Science
Aston University, Birmingham, United Kingdom, B4 7ET
Email: y.zhang10@aston.ac.uk
(Corresponding author)

[1] This is an Accepted Manuscript of an article to be published by *International Journal of Fatigue*. Access to the full text of the paper is available at https://doi.org/10.1016/j.ijfatigue.2020.105738

Abstract:

This study aims to model fatigue crack initiation in bituminous binders. An energy-based crack initiation criterion is developed for bitumen under a rotational shear fatigue load. Based on a damage mechanics analysis of fatigue cracking process, the crack initiation is defined and local energy redistribution around crack tips due to 'factory-roof' cracking is quantified. A quantitative energy criterion is proposed for the fatigue crack initiation in the bitumen using viscoelastic Griffith's theory. The crack initiation criterion is validated through comparing the predicted and measured surface energy of the bitumen. The results show that bitumen fatigue cracking under the rotational shear fatigue load can be divided into two stages: the edge flow damage and the 'factory-roof' cracking. The crack initiation is dependent of the shear modulus and surface energy of bituminous binders, critical crack size, and loading amplitude. The energy-based crack initiation criterion along with the DSR fatigue tests can be potentially used to determine the material surface energy.

Key words:

Dynamic shear rheometer (DSR); time sweep; energy-based crack initiation criterion; viscoelastic Griffith's theory; surface energy

1. Introduction

Fatigue cracking in bituminous binders is one of the most major distresses resulting in the degradation of asphalt pavements. To optimise the material selection and consequently improve the pavement performance, research efforts have been made to characterise and quantify the fatigue performance of the bituminous binders. Based on Dynamic Shear Rheometer (DSR) tests, a number of fatigue parameters were proposed to evaluate the fatigue resistance of the binders, including SHRP fatigue factor $|G^*|\cdot\sin\delta$, dissipated energy ratio (DER) [1-3], ratio of dissipated energy change (RDEC) [4-7] and fatigue law based on the viscoelastic continuum damage (VECD) mechanics [8-12]. Although these fatigue parameters have been employed to characterise the binders' fatigue behaviour, the fatigue cracking mechanism of the bituminous binders are not yet well understood, particularly on how the crack was initiated in the binders under a rotational shear fatigue load. Further studies from the fundamental mechanical perspective are very needed to understand the initiation of the fatigue damage for the bituminous binders under the shear fatigue load.

Three key questions have been raised by the authors as follows: (a) what the damage looks like in the bituminous binder under the shear fatigue load; (b) when the damage is initiated; and (c) how the damage evolves. The question (a) on what the damage is has been tentatively addressed by one of the authors' previous studies [13]. It was found that the fatigue damage in the bituminous binders under the rotational shear fatigue loads physically exhibited as an edge cracking, which was a circumferential crack that initiated at the edge of the sample and propagated toward the centre. The cracked surfaces in the bitumen samples after the rotational shear fatigue load are demonstrated as roughed 'factory-roof' like surfaces, which were also observed and characterised by the existing studies [13, 14]. Using damage mechanics, a DSR-cracking (DSR-C) model was developed to predict the crack length in the bitumen sample under the rotational shear fatigue load [13]. In the DSR-C model, the crack length can be calculated using the shear moduli and phase angles of the bitumen at the undamaged and damaged conditions, respectively. The proposed DSR-C model is proven to be capable of accurately predicting the crack length for the unaged and aged virgin or modified bituminous binders in the DSR fatigue testing (e.g., time sweep test) at different temperatures, loading frequencies and cycles. Based on the analysis of fatigue cracking process with the DSR-C model, the question (c) on how the damage crack evolves has also been investigated using pseudo J-integral Paris' law in a separate work [15]. It was found the model coefficients (A and n) from the Paris' law are material fundamental properties, which are function of temperature but independent of loading frequency or loading amplitude. A similar finding was reported for asphalt mixtures [16, 17].

Following the understanding of the first and third questions, this study is focused on addressing the second question that is when the damage is initiated. Crack initiation refers to the onset of edge cracking, which is critical to estimate the crack propagation and fatigue life in a material under a cyclic load. Based on the microscopic observations, a number of studies have been carried out for metals and polymers to elucidate the mechanisms of crack initiation. It was found that the crack initiation of metallic materials is mainly caused by dislocations [18]. According to the dislocation movement and plastic deformation, dislocation-based models were proposed to characterise the crack initiation in the metallic materials [19-21]. Polymeric materials are composed of molecular chains, which present a viscoelastic fracture. Its crack initiation results from the chain scission or chain disentanglement. The plastic zone-based model [22, 23] or craze zone-based models [24-26] were developed to investigate the crack initiation of polymeric materials. Furthermore, the local crack growth models were proposed for viscoelastic materials, which provide the analytical solutions to crack initiation problems. Knauss [27] developed a crack speed criterion for viscoelastic materials by defining a critical crack speed transition using continuum mechanics. Schapery [28] defined a crack tip model with a failure zone behind the tip and developed a local energy criterion for viscoelastic materials to predict the time of crack initiation. While these models can be used to analyse the process of crack initiation, their application in engineering practice, e.g., asphalt mixtures, is limited due to complexity in the determination of the model inputs and the validations of the model predictions.

Griffith's energy criterion presented a more general manner to predict the crack initiation, which defined the energy condition at which the crack is initiated in brittle materials [29]. Recently, Griffith's crack initiation theory has been extended to develop a fracture criterion for the viscoelastic materials [30-32]. The viscoelastic Griffith's criterion states that the potential energy of a viscoelastic body remains at equilibrium when cracks initiate. Dubois and Petit [33] used the viscoelastic Griffith's criterion to investigate the effects of viscoelastic characteristics on the creep crack initiation by developing a path-independent integral $G\theta_v$. Luo, Luo and Lytton [34] and Zhang, Luo, Luo and Lytton [35] applied viscoelastic Griffith's criterion to develop the crack initiation criteria for the asphalt mixtures in tension and compression, respectively. The tensile crack initiation criterion results in a simple way of measuring the endurance limit and the compressive one leads to a simple way of predicting compressive strength [36]. These researches have demonstrated that the viscoelastic Griffith's criterion is capable of characterising the crack initiation of the viscoelastic materials. In this study, the viscoelastic Griffith's criterion will be employed to investigate the crack initiation for the bituminous binders under the rotational shear fatigue loads.

The objective of this study is to develop an energy-based crack initiation criterion for the bituminous binders subjected to a rotational shear fatigue load. Laboratory tests including contact angle measurements and DSR tests were firstly conducted, which are followed by the viscoelastic characterisation of bituminous binders using the pseudostrain concept. Based on the analysis of the fatigue cracking process, crack initiation was defined and energy redistribution due to 'factory-roof' cracking was illustrated. Subsequently, an energy criterion for crack initiation was proposed and validated for bituminous binders under the rotational shear fatigue load using the viscoelastic Griffith's fracture mechanics. Finally, a potential application of the crack initiation criterion was presented, which is to determine the surface energy of the bituminous binders.

2. Materials and Laboratory Tests

2.1 Materials

Four types of bituminous binders were applied in this study, including 40/60 bitumen, X-70 bitumen, base X-70 bitumen and 100/150 bitumen. The 40/60 bitumen, base X-70 bitumen and 100/150 bitumen are unmodified binders with different penetration grades and the X-70 bitumen is a polymer-modified binder with 45/80 penetration grade.

These binders were all aged using standard methods including Rolling Thin Film Oven (RTFO) for short-term ageing [37] and Pressure Ageing Vessel (PAV) for long-term ageing [38]. Laboratory tests including contact angle measurements and Dynamic Shear Rheometer (DSR) tests were conducted on eight samples, i.e., unaged 40/60 bitumen, RTFO aged 40/60 bitumen, PAV aged 40/60 bitumen, unaged X-70 bitumen, RTFO aged X-70 bitumen, PAV aged X-70 bitumen, PAV aged base X-70 bitumen and PAV aged 100/150 bitumen.

2.2 Contact angle measurements

In order to determine surface energy of the bituminous binders, contact angle measurements were performed using Sessile Drop method. This method provides a standard test for surface properties of solids and liquids, which has been widely applied for the study of the surface energy of bituminous binders [39-41]. In the Sessile Drop method, contact angles between probe liquids and bitumen sample are measured directly by capturing an image of a liquid drop on the sample surface.

The selection of probe liquids is critical for the contact angle measurements using the Sessile Drop method. The used liquids first need to be pure, homogenous and immiscible with the bituminous binders. Their surface energy components must be known to determine the surface energy of bituminous binders. In this study, distilled water, ethylene glycol and formamide were selected from the literature [41] as probe liquids for the contact angle experiments. Surface energy characteristics of the three probe liquids are summarized in **Table 1**. The magnitudes of their surface energy components are very distinctive, which is advantageous to accurately calculate the surface energy of bituminous binders later. The bitumen samples used for the contact angle measurements were prepared using glass slides with 25 mm × 75 mm × 1 mm in size, as shown in **Fig. 1(a)**. A small quantity of the heated bitumen was poured on a clean glass slide to form a bitumen substrate with a flat and smooth surface. The bitumen sample was cooled to room temperature before the contact angle measurements. Note that three coated slides for each bitumen are needed for three probe liquids.

Table 1 Surface energy components of probe liquids (mJ/m^2).

Liquids	Γ	Γ^{LW}	Γ^{+}	Γ^{-}
Distilled Water (W)	72.80	21.80	25.50	25.50
Ethylene Glycol (EG)	48.00	29.00	1.92	47.00
Formamide (F)	58.00	39.00	2.28	39.60

Once the probe liquids were selected and the bitumen samples were prepared, the contact angle measurements were conducted using an optical tensiometer from Biolin Scientific shown in **Fig. 1(b)**. The glass slide coated with the bitumen was first placed between the light source and the camera of the test device. A small drop of the probe liquid was dispensed on the surface of the coated slide. An image of the drop was captured by the camera and then the captured image was analysed automatically by image processing software of the test device to obtain the angle between the baseline and the edge of the drop. Five measurements were performed for each probe liquid. Their average value was determined as the contact angle between the probe liquid and the bitumen. **Table 2** shows the results of the contact angle measurements for all tested bituminous binders. Based on the measured contact angles, the surface energy of the bituminous binders can be calculated using the Good-van Oss-Chaudhury theory [42], which will be discussed in detail later.

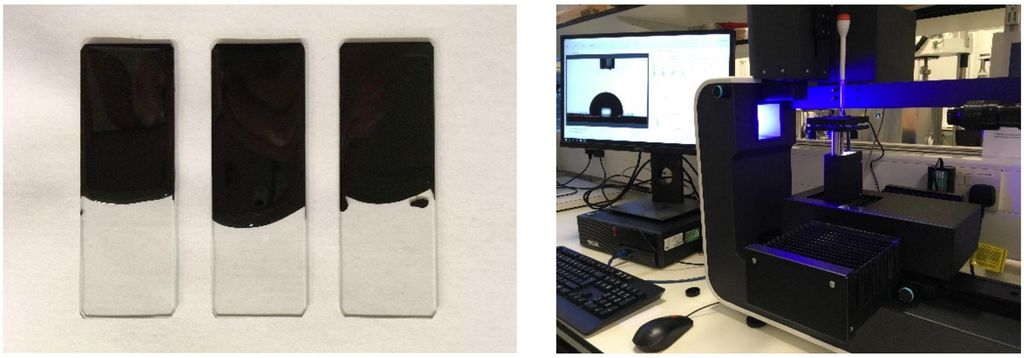

(a) (b)

Fig. 1. Bitumen samples and test instrument used for contact angle measurements. (a) Glass slide samples. (b) Tensiometer from Biolin Scientific.

Table 2 Contact angles between tested bitumen and liquid probes (°).

Bitumens	Distilled Water (W)	Ethylene glycol (EG)	Formamide (F)
Unaged 40/60	105.68±0.62	82.43±0.29	90.17±0.73
RTFO 40/60	103.80±0.18	81.98±0.80	89.44±0.64
PAV 40/60	107.09±0.37	81.77±0.93	91.45±0.65
Unaged X-70	104.10±0.39	79.59±0.45	89.04±0.58
RTFO X-70	101.57±1.42	80.87±0.49	88.85±1.66
PAV X-70	103.37±0.68	81.86±0.30	92.05±0.82
PAV base X-70	103.80±0.14	80.74±0.67	88.16±0.82
PAV 100/150	103.21±0.35	80.82±0.63	88.90±0.45

2.3 Dynamic Shear Rheometer (DSR) tests

To determine the linear viscoelastic properties and fatigue cracking behaviours of the bituminous binders, viscoelastic frequency sweep tests and time sweep fatigue tests were performed on all binders in this study. Bitumen samples were prepared for the tests using silicone moulds and all the tests were conducted using a Kinexus DSR from Malvern Panalytical with an 8 mm parallel plates with 2 mm gap as the sample height. Before the bitumen samples were subjected to the testing load, they were heated to the target temperature and then remained 5 min to allow temperature equilibrium and material stability. Two replicates were tested for each testing condition and one more replicate was required when their deviation was more than 10%.

To eliminate the effects of the initial stiffness of the bituminous binders, a fixed iso-stiffness level at which $|G^*| \cdot \sin\delta$ equals to 6.5 MPa at 10 Hz were used to determine testing temperatures. Frequency sweep tests at multiple temperatures from 10 ℃ to 40 ℃ were conducted to obtain the corresponding temperature for each tested sample. The temperatures resulted from the iso-stiffness condition range from approximately 15 ℃ to 35 ℃, as shown in **Table 3**. It should be noted that the iso-stiffness temperature is different for each tested binder in the following time sweep fatigue test. The shear modulus ($|G_0^*|$) and the phase angle (δ_0) of the undamaged binder can be obtained from the frequency sweep test conducted at the iso-stiffness temperature.

Table 3 Iso-stiffness temperature for all the tested bitumens.

Bitumens	Iso-stiffness temperature (°C)
Unaged 40/60	24
RTFO 40/60	27
PAV 40/60	34
Unaged X-70	21
RTFO X-70	24
PAV X-70	28
PAV base X-70	28
PAV 100/150	26

To study the fatigue cracking behaviours of the binders, time sweep fatigue tests were performed at the iso-stiffness temperature and the frequency of 10 Hz under a 5% shear strain level corresponding to the rotation amplitudes of 0.025 rad. The strain level (5%) have been employed for time sweep fatigue tests in the literature [13, 43] to investigate the fatigue damage response of bituminous binders. **Fig. 2** illustrates a typical result of the time sweep test for a PAV aged X-70 bitumen sample.

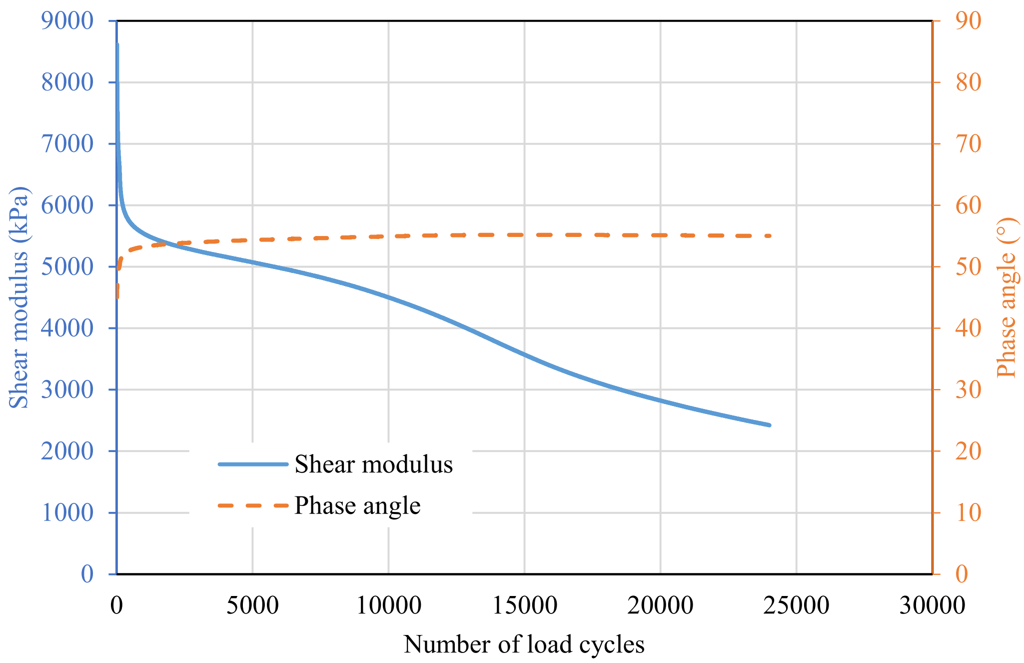

Fig. 2. Time sweep test results for a PAV aged X-70 bitumen sample at 28 °C.

3. Viscoelastic characterisation of bituminous binders with pseudostrain

When a viscoelastic material is subjected to a rotational shear fatigue load, its stress-strain curve forms a hysteresis loop in each load cycle. The area inside the loop is the dissipated strain energy (DSE) density and the area between the stress-strain curve and the horizontal (strain) axis is defined as the recoverable strain energy (RSE) density. The DSE for the materials in the linear viscoelastic undamaged state is the energy dissipated due to the viscoelastic relaxation of the material. In order to remove the viscous effect, pseudostrain was proposed by Schapery [44] below

$$\gamma^{R}(t)=\frac{1}{G_{R}}\int_{0^{-}}^{t}G(t-s)\frac{d\gamma(s)}{ds}ds \tag{1}$$

where γ^{R} is the pseudostrain; G_{R} is the shear reference modulus; $G(t)$ is the shear relaxation modulus; s is the time before the current time t; and $\gamma(s)$ is the measured total strain. Pseudostrain has been used in the damage characterization of asphalt mixtures [16, 35, 45-47]. After introducing pseudostrain, the stress-pseudostrain curve at the linear viscoelastic state becomes a straight line, which indicates that the viscous effect is eliminated and the stress-pseudostrain shows like an elastic behaviour. The area below the stress-pseudostrain curve is the recoverable pseudostrain energy (RPSE) density. RPSE is the density of the energy stored in the material during loading and can be released during unloading, which is used for crack initiation analysis of the bituminous binders under rotational a shear fatigue load in this study.

In a strain-controlled rotational shear fatigue test (e.g., time sweep test) of a cylindrical bitumen sample, the applied shear strain is

$$\gamma(t)=\gamma_{0}\sin(\omega t) \tag{2}$$

where γ_{0} is the strain amplitude and ω is the loading frequency. The strain amplitude at a given radial position of the sample is expressed as

$$\gamma_{0}(r)=\frac{\theta_{0}}{h}\cdot r \text{ with } 0\leq r\leq r_{0} \tag{3}$$

where θ_{0} is the controlled amplitude of rotational angle, r_{0} and h are the original radius and the height of the cylindrical sample, respectively. Thus, in the strain-controlled cyclic test, the pseudostrain $\gamma^{R}(t)$ in **Eq. (1)** at the linear viscoelastic condition can be determined as

$$\gamma^{R}(t)=\frac{\gamma_{0}}{G_{R}}\left|G_{0}^{*}\right|\sin(\omega t+\delta_{0}) \tag{4}$$

where δ_0 is the phase angle of the material in the undamaged condition. The corresponding pseudostrain amplitude is written as

$$\gamma_0^R = \frac{\gamma_0}{G_R}\left|G_0^*\right| \tag{5}$$

Based on the definition of RPSE density that is the area between the stress-pseudostrain curve and the horizontal (pseudostrain) axis, the value of RPSE density at a given radial position of the sample at the linear viscoelastic condition can be calculated as

$$RPSE(r) = \frac{1}{2}\tau_0 \cdot \gamma_0^R \tag{6}$$

where τ_0 is the amplitude of the measured shear stress corresponding to the controlled shear strain $\gamma(t)$ shown in **Eq. (2)**. According to the linear viscoelastic stress-strain law, the shear stress amplitude of the sample can be obtained by

$$\tau_0 = \left|G_0^*\right|\gamma_0 = G_R\gamma_0^R \tag{7}$$

Substituting **Eqs. (5)** and **(7)** into **Eq. (6)** and considering **Eq. (3)**, RPSE density at a given radial position of the cylindrical bitumen sample can be given as

$$RPSE(r) = \frac{1}{2}\frac{\left(\left|G_0^*\right|\theta_0\right)^2}{G_R h^2} \cdot r^2 \tag{8}$$

From **Eq. (8)**, one can find that the RPSE density is non-uniform along the radial direction of the cylindrical bitumen sample but a quadratic function of the radius r for the sample. The maximum RPSE occurs at the location where the radius is the maximum which is the edge of the sample. This again proves that the crack tends to be initiated from the edge of the sample.

4. Crack initiation modelling of bituminous binders

4.1 Crack initiation of bituminous binders under a rotational shear fatigue load

Under a rotational shear fatigue load, the crack in a cylindrical bitumen sample grows as a circumferential crack that initiates at the edge of the sample and propagates toward the centre [13, 14]. A typical crack surface in the bitumen samples is shown in **Fig. 3(a)**. It can be seen that the crack surface exhibits three different zones based on the morphology of the cracking surfaces:

1) Edge flow zone. The damage at the edge flow zone is known as 'edge flow' that occurs at the edge of the sample and at the initial stage of fatigue cracking. The edge flow is caused by edge instability with complex mechanisms.
2) 'Factory-roof' cracking zone. At the 'factory-roof' cracking zone, the crack is a single ring crack that steadily propagates towards the centre of the sample, resulting in a rough and 'factory-roof' like cracking surface under the shear-mode loading.
3) Uncracked zone. The uncracked zone is the zone in the sample centre which is not damaged during the rotational shear fatigue load. However, it is generated and captured by pulling the top and bottom sample apart after the fatigue test at a relatively low temperature (i.e., 3 °C). The low-temperature is used to conserve the configuration of the crack surfaces including flow zone crack and the 'factory-roof' crack generated during the fatigue test.

Thus, bituminous binders' fatigue cracking under the rotational shear fatigue load can be divided into two stages: edge flow damage and 'factory-roof' cracking. **Fig. 3(b)** shows the schematic side view of a cylindrical sample with a circumferential crack.

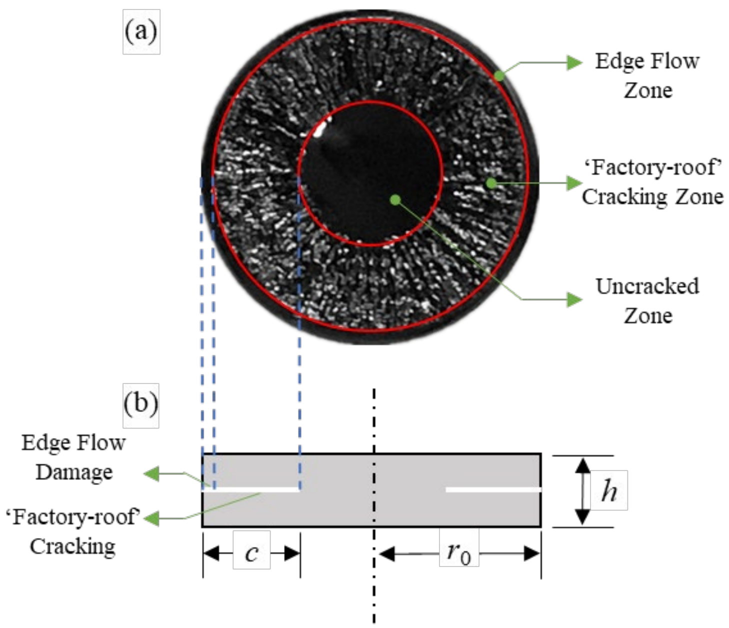

Fig. 3. Fatigue cracking in bituminous binders under a rotational shear fatigue load. (a) Cracking morphology. (b) Cracking model. c is the crack length, r_0 is the original radius of the sample, and h is the height of the sample.

Based on the DSR-C model shown in **Eq. (9)** [13], the crack growth in bituminous binders under a rotational shear fatigue load can be predicted using the moduli and phase angles of the binders in the undamaged and damaged conditions.

$$c = \left[1 - \left(\frac{|G_N^*| / \sin(\delta_N)}{|G_0^*| / \sin(\delta_0)} \right)^{\frac{1}{4}} \right] r_0 \tag{9}$$

where c is the crack length in the cylindrical bitumen sample; $|G_0^*|$ and δ_0 are the shear modulus and the phase angle in the undamaged condition, respectively; $|G_N^*|$ and δ_N are the shear modulus and the phase angle at the Nth load cycle in the damaged condition, respectively; and r_0 is the original radius of the bitumen sample.

Fig. 4 shows a typical crack growth curve with the number of load cycles, determined using **Eq. (9)**. The corresponding crack growth rate with the crack length is plotted in **Fig. 5**. It is very clear from **Figs. 4** and **5** that, before the 1000th load cycle, the crack growth rate is decreasing but still much higher than that after the 1000th load cycle. When the load cycle goes beyond the 1000th load cycle or the crack length is greater than 0.55 mm, the crack presented a regular growth in a relatively lower growth rate kept decreasing. This crack growth stage is referred to as the crack propagation ('factory-roof' cracking), which has been studied in the previous work [15]. Before the crack propagation stage, the initial portion of fatigue cracking is believed as the edge flow damage.

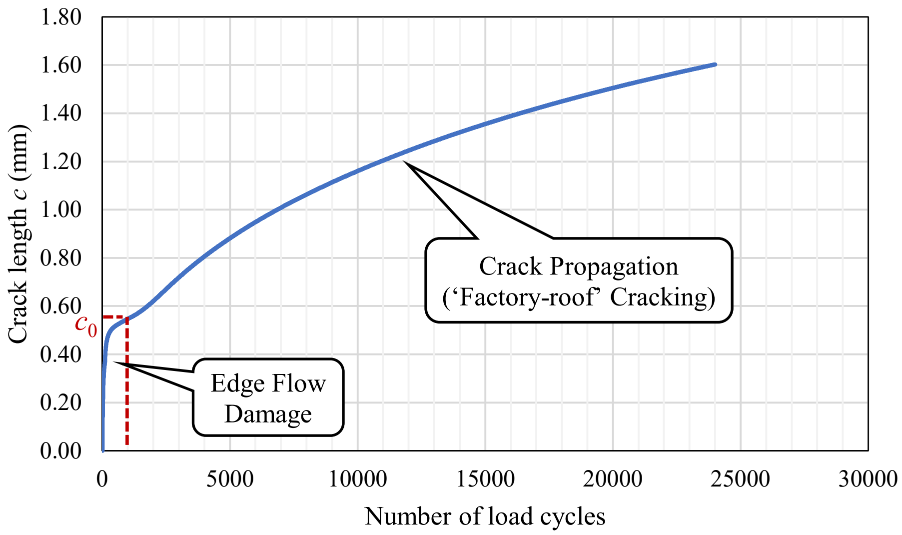

Fig. 4. Crack growth with the number of load cycles for a cylindrical bitumen sample subjected to a rotational shear fatigue load.

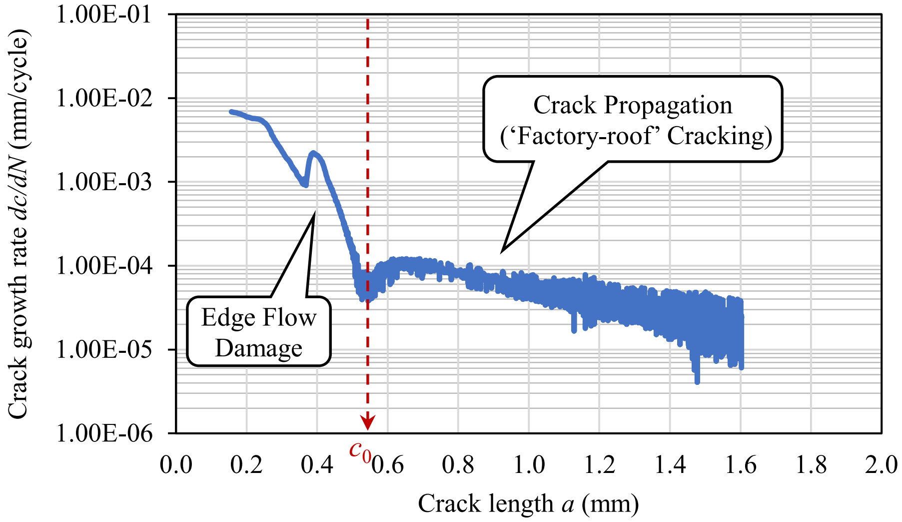

Fig. 5. Crack growth rate with the crack length for a cylindrical bitumen sample subjected to a rotational shear fatigue load.

Edge flow damage is an unsteady cracking stage with complex cracking mechanisms. It can be seen from **Figs. 4** and **5** that the crack length has a sharp increase and the crack growth rate shows a significant fluctuation. A sequence of processes occurring in this stage are described as follows:

(1) Molecular rearrangements. When the bituminous binders are subjected to the

external rotational shear fatigue load, their physical properties such as shear modulus and phase angle changes rapidly (see **Fig. 2**). This phenomenon is caused by the rearrangement of molecular chains in binders [48, 49], which is referred to as the thixotropic effect [50].

(2) Microcrack nucleation. After the molecular rearrangements, the microcracks are initiated at the edge of cylindrical bitumen sample either by the breakage of atomic bonds or from the pre-existing vacancies and flaws in the materials. These microcracks then occur nucleation and form small macrocracks [51].

(3) Circumferential crack formation. With the increasing load cycles, small macrocracks are eventually interconnected to generate a single circumferential crack at the edge of sample. The initial circumferential crack length c_0 is defined as the edge flow damage size which separates the crack growth rate into completely two different stages. As shown in **Fig. 5**, the crack growth rate is much higher but drops much quicker in the edge flow damage stage than that in 'factory-roof' crack propagation stage.

Due to the edge instability and geometry dependence of samples, it becomes very challenging to develop a rigorous model or theory to characterise the molecular rearrangements or the microcrack nucleation during the edge flow damage. However, after the circumferential crack formation, the 'factory-roof' crack propagates at a relatively stable and more consistent manner as shown in **Figs. 4** and **5**. Thus in this study the "crack initiation" is defined as the moment at which the circumferential crack formation is complete, which is also the end of the edge flow damage and the start of the 'factory-roof' crack propagation. **Fig. 6** is proposed to model the crack initiation, at which the edge flow damage stage has been finished, thus the crack size has reached a length of c_0.

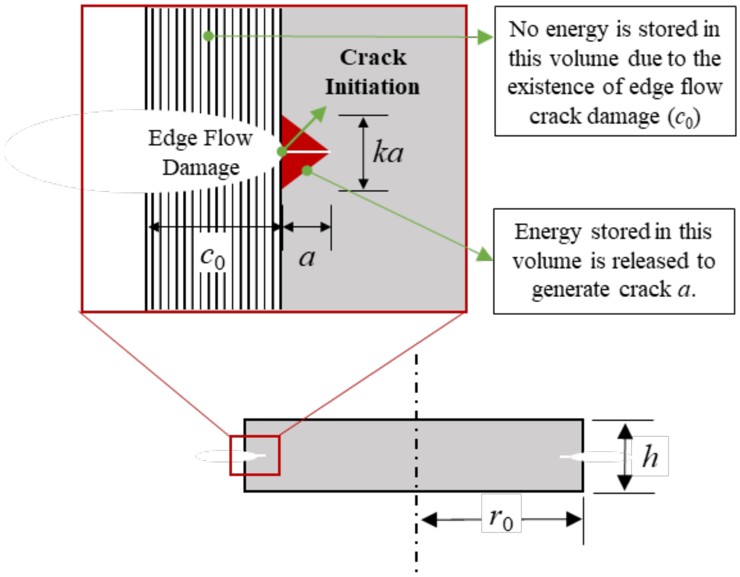

Fig. 6. Edge flow damage and crack initiation of 'factory-roof' cracking zone. c_0 is the edge flow damage size. a is the 'factory-roof' crack length for crack initiation.

4.2 Energy redistribution due to 'factory-roof' cracking

Cracking is a process of energy redistribution in material according to Griffith theory. For bituminous binder, a viscoelastic material, pseudostrain is applied to replace the physical strain so that a viscoelastic problem could be simplified as an elastic one.

According to the cracking pattern of bitumen binders under the rotational shear fatigue load shown in **Figs. 3** and **6,** the total RPSE in bitumen sample with the edge flow damage is redistributed due to the appearance of the circumferential 'factory-roof' crack as follows: (1) RPSE is released from the intact material surrounding the 'factory-roof' crack and (2) surface energy is stored on the surfaces of the 'factory-roof' crack. Thus, the energy redistribution resulting from the 'factory-roof' cracking is formulated as

$$\varepsilon = \varepsilon_1 - \varepsilon_2 + \varepsilon_3 \tag{10}$$

where ε is the total pseudostrain energy after the energy redistribution in the cylindrical bitumen sample; ε_1 is the total RPSE in the sample with the edge flow damage before the circumferential 'factory-roof' crack initiates; ε_2 is the released RPSE surrounding the circumferential 'factory-roof' crack; and ε_3 is the total surface energy stored on the ‘factory-roof’ crack surfaces.

To analyse the energy redistribution in bitumen sample, the three energy elements (ε_1, ε_2 and ε_3) were further derived based on the cracking model of bitumen sample shown in **Fig. 6**. The total RPSE in the sample with the edge flow damage before the ‘factory-roof’ crack initiates (i.e., ε_1) is defined as

$$\varepsilon_1 = \iiint_{V_{total}} RPSE(r)dV = \int_0^{r_0-c_0} RPSE(r)\cdot(2\pi rh)\,dr \tag{11}$$

where V_{total} is the volume of the sample except the edge flow damage zone (the vertically shaded part shown in **Fig. 6**). Note that the edge flow damage zone was removed from the calculation of the V_{total} as no RPSE was stored in the zone due to the edge flow damage in the sample.

The released RPSE surrounding the ‘factory-roof’ crack (i.e., ε_2) is calculated as

$$\varepsilon_2 = \iiint_{V_{relesaed}} RPSE(r)dV \approx RPSE(r)\cdot V_{relesaed} \tag{12}$$

where $V_{released}$ is the volume of the sample that releases RPSE to generate the ‘factory-roof’ crack. As shown in **Fig. 6**, when a very small ‘factory-roof’ crack a ($a \ll c_0$) is initiated, only the energy stored in the adjacent volume of the crack is released. It was assumed that this volume is a triangular ring region and highlighted as the red area as shown in **Fig. 6**. A similar assumption was used in the crack initiation modelling in rubber [52] and asphalt mixtures [34]. The horizontal height of the triangular region is the crack length a and the vertical height of the triangular region is ka according to the previous study [52]. Thus, the volume for releasing RPSE can be expressed as

$$V_{released} = \frac{1}{2}\cdot ka\cdot a\cdot 2\pi(r_0 - c_0) \tag{13}$$

The total surface energy stored on the 'factory-roof' crack surfaces ε_3 is determined as

$$\varepsilon_3 = \Gamma \cdot 2A = \Gamma \cdot 2\left[\pi\left(r_0 - c_0\right)^2 - \pi\left(r_0 - c_0 - a\right)^2\right] \tag{14}$$

where Γ is the total surface energy of the bituminous binders that is the energy (or work) done to create a unit area of the new surface; A is the surface area of a circumferential crack; and the coefficient 2 refers to that every crack has two surfaces.

4.3 Crack initiation criterion

The Griffith crack initiation criterion states that the potential energy of an elastic body remains unchanged when cracks initiate or the existing cracks grow. Thus, the crack initiation follows an energy balance condition, where the rate of total energy to crack size equals to zero. Based on this criterion, the critical condition at the moment when the crack is initiated can be expressed as

$$\frac{\partial \varepsilon}{\partial c} = 0 \tag{15}$$

where ε is the total pseudostrain energy after the energy redistribution in the sample shown in **Eq. (10)**. Then, substituting **Eq. (10)** with **Eqs. (11)**, **(12)**, **(13)**, and **(14)** into **Eq. (15)** and performing differentiation give

$$RPSE\left(r\right) \cdot k \cdot a \cdot \left(r_0 - c_0\right) - 2\Gamma \cdot \left(r_0 - c_0 - a\right) = 0 \tag{16}$$

Eq. (16) is the energy-based crack initiation criterion for bituminous binders under the rotational shear fatigue load. It is noted that, in **Eq. (16)**, the recoverable pseudostrain energy density *RPSE*(*r*) is related to the shear modulus of materials and the loading amplitude (see **Eq. (8)**). Thus, the energy-based crack initiation criterion (**Eq. (16)**) shows that the crack initiation is dependent of the shear modulus and surface energy of bituminous binders, critical crack size, and loading amplitude.

5. Results and discussions

5.1 Surface energy of bituminous binders

Surface energy of a material is defined as the energy required to create a unit area of the new surface in the material. According to the acid-base theory [53], the total surface energy of a material is mainly comprised of a nonpolar Lifshitz-van der Waals (LW) component and an acid-base (AB) component, as expressed in **Eq. (17)**.

$$\Gamma = \Gamma^{LW} + \Gamma^{AB} \tag{17}$$

where Γ is the total surface energy, Γ^{LW} is the Lifshitz-van der Waals (LW) component, and Γ^{AB} is the acid-base component.

To predict the acid-base interaction, the acid-base term in **Eq. (17)** was divided into a Lewis acid component and a Lewis base component, as described in **Eq. (18)**.

$$\Gamma^{AB} = 2\sqrt{\Gamma^{+}\Gamma^{-}} \tag{18}$$

where Γ^{+} is the Lewis acid surface parameter and Γ^{-} is the Lewis base surface parameter.

The surface energy components of the bituminous binders were determined indirectly using contact angle measurements in this study. **Table 2** shows the contact angles between bitumen and three liquid probes. Based on the contact angle values, the surface energy components (Γ_S^{LW}, Γ_S^{+} and Γ_S^{-}) of bitumen can be obtained by the Young-Dupre equation shown in **Eq. (19)** [54].

$$(1+\cos\theta)\Gamma_L = 2\left(\sqrt{\Gamma_S^{LW}\Gamma_L^{LW}} + \sqrt{\Gamma_S^{+}\Gamma_L^{-}} + \sqrt{\Gamma_S^{-}\Gamma_L^{+}}\right) \tag{19}$$

where θ is the contact angle between bitumen (S) and probe liquid (L).

Once the surface energy components (Γ_S^{LW}, Γ_S^{+} and Γ_S^{-}) of bitumen were obtained, the total surface energy of bitumen was determined using **Eqs. (17)** and **(18). Table 4** shows the total surface energy of the tested binders with their surface energy components.

Table 4 Surface energy components of tested bitumens (mJ/m^2).

Bitumens	Γ	Γ^{LW}	Γ^{AB}	$\sqrt{\Gamma^{+}}$	$\sqrt{\Gamma^{-}}$
Unaged 40/60	11.51	8.15	3.37	1.49	1.13
RTFO 40/60	12.56	8.79	3.77	1.39	1.36
PAV 40/60	8.89	4.80	4.09	2.08	0.98
Unaged X-70	10.80	5.98	4.82	1.96	1.23
RTFO X-70	12.91	7.93	4.98	1.51	1.65
PAV X-70	10.59	3.48	7.11	2.21	1.61
PAV base X-70	13.11	9.73	3.39	1.36	1.24
PAV 100/150	12.32	7.99	4.33	1.56	1.39

5.2 Determination of model parameters

To implement the energy-based crack initiation criterion for the bitumen in **Eq. (16)**, the model parameters are discussed and determined in this section. The recoverable pseudostrain energy density *RPSE*(r) is calculated using **Eq. (8)** with the crack initiation position $r = r_0 - c_0$. More specifically, the shear modulus $|G_0^*|$ in the undamaged condition is obtained from the frequency sweep tests. The controlled amplitude of rotational angle θ_0 is 0.025 rad. The shear reference modulus G_R is determined as the shear modulus $|G_0^*|$. The authors' previous study [45] proved that, when assigning the material modulus to the reference modulus, the physical meaning of the pseudostrain becomes the difference between the viscous strain and the total strain. It is noted that some studies [55, 56] used a unit (1 Pa) as the reference modulus, however, this will result in an unclear physical meaning of the pseudostrain as the unit reference modulus has normalised the pseudostrain when the stress-pseudostrain relations are modelled.

The surface energy Γ was calculated based on the contact angle measurements that have been presented in **Section 5.1**. The edge flow damage size c_0 was determined as the corresponding crack length at which the minimum crack growth rate was obtained before the "factory-roof" crack propagation is started in the TS tests, as shown in **Fig. 5**. The radius r_0 and the height h of the cylindrical bitumen sample were 4 mm and 2 mm, respectively.

The coefficient k of the vertical height ka in the triangular region shown in **Fig. 6** is determined as 2π [34]. Note that the 'factory-roof' crack length $a << c_0$ at the critical moment of the crack initiation, thus it is assumed that the crack length $a = \alpha \cdot c_0$ where α is within a range from 0.0004 to 0.0012 for the tested bitumen samples. It is noted that the triangular region that releases the RPSE is strongly related to the material viscoelastic property, leading to the small difference in the values of the parameter α for the different bituminous binders. It is very challenging to directly measure the parameter α in the lab tests due to the critical moment of the fatigue crack initiation.

5.3 Validation of crack initiation criterion

To validate the crack initiation criterion, **Eq. (16)** is used to predict the surface energy of the bitumen. Based on **Eq. (8)**, *RPSE*(r) at the crack initiation position $\left(r_0 - c_0\right)$ is written as

$$RPSE = \frac{1}{2}\frac{\left(\left|G_0^*\right|\theta_0\right)^2}{G_R h^2}\cdot\left(r_0 - c_0\right)^2 \tag{20}$$

Then, substituting **Eq. (20)** into **Eq. (16)** and using $r_0 - c_0 - a \approx r_0 - c_0$ due to $a << c_0$ for the crack initiation, the surface energy of the bitumen can be calculated by

$$\Gamma = \frac{\left(\left|G_0^*\right|\theta_0\right)^2 \cdot k \cdot a \cdot \left(r_0 - c_0\right)^2}{4 G_R h^2} \tag{21}$$

Fig. 7 presents the comparison between the calculated results from **Eq. (21)** and the tested results shown in **Table 3**. The quality line ($y = x$) is added in Fig.7 to clearly show the difference between the predicted and measured results. Closer the data points are to the quality line, smaller the difference between the predicted and measured values is. The difference ratio R is also calculated to show a measure of how close the data are to the quality line. It is defined as the absolute difference between the predicted and measured values divided by the measured value. The average R for all tested samples is 7.51%, which means that the predicted results agree well with the tested data. Thus, the energy-based crack initiation criterion is validated for all the tested bituminous binders. Furthermore, it is concluded that the crack initiation criterion can be used to determine the surface energy of the bituminous binders by the DSR fatigue tests.

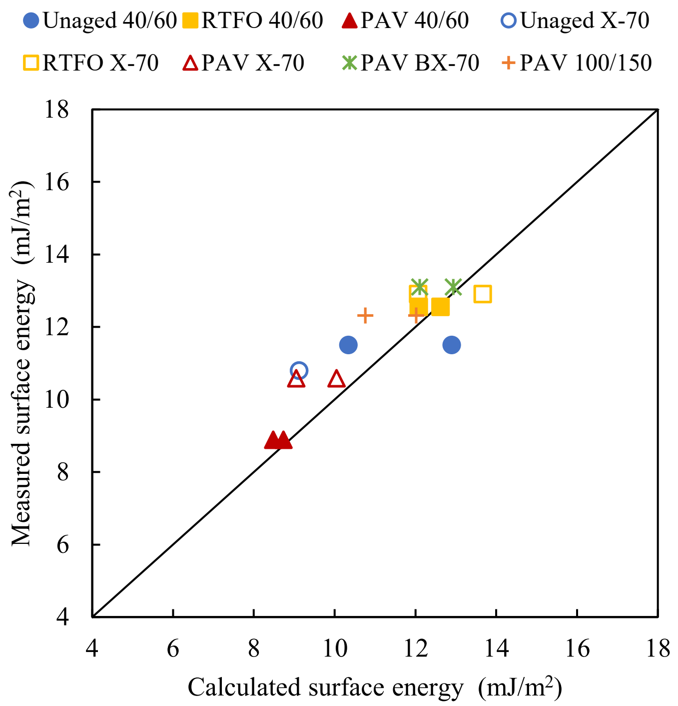

Fig. 7. Comparison between the calculated results and the tested data from the contact angle measurements.

5.4 Crack initiation analysis of bituminous binders

After validation, the fatigue crack initiation of bituminous binders can be analysed using the developed energy-based criterion. In this study, eight types of bituminous binders are tested, including the unmodified and polymer-modified samples under the unaged and aged conditions. The experimental results of DSR fatigue tests are presented, including the shear modulus and phase angle (**Fig. 2**), cracking morphology

(**Fig. 3**), crack length (**Fig. 4**), and crack growth rate (**Fig. 5**). According to these experimental results, the fatigue cracking process in the bituminous binders is analysed and discussed to reveal the cracking mechanism and thus to model the fatigue crack initiation illustrated in **Fig. 6**. Based on the cracking mechanism and the developed criterion (**Eq. (16)**), the edge flow damage size c_0, the 'factory-roof' crack length a and the number of load cycles to initiation are calculated and presented in **Table 5** for all tested bituminous binders.

It can be seen from **Table 5** that the polymer-modified X-70 bitumen exhibits a smaller edge flow damage size than the unmodified 40/60 bitumen in the unaged or aged condition, indicating a better resistance to the edge flow damage. The edge damage size for both the 40/60 and X-70 binders increases with the increasing ageing level, which means that the ageing can accelerate the edge flow damage. At the moment of circumferential crack initiation, the 'factory-roof' crack length is found within one micrometre for all tested bituminous binders. It is suggested that the microscopic damage in the bituminous binders subjected to the rotational shear fatigue loads needs to be examined and explored to understand the role of microstructure in the fatigue crack initiation.

Table 5 also shows the number of load cycles until crack initiation for the tested binders. For both the 40/60 and X-70 binders, the number of load cycles grows as the ageing level increases. This is because that the aged binders have a greater shear modulus. However, a higher value of load cycles to crack initiation does not means a longer fatigue life that consists of not only the crack initiation life but also the crack propagation life. It has been reported by the authors' previous study [15] that the ageing accelerates the crack propagation and reduce the fatigue crack propagation life. Among the four kinds of PAV aged binders (i.e., PAV 40/60, PAV X-70, PAV base X-70, PAV 100/150), the number of load cycles for the polymer-modified X-70 bitumen is the largest (4314), which demonstrates that the polymer modification can improve the binder resistance to the crack initiation and extend the fatigue crack initiation life.

Table 5 Predicted results of fatigue crack initiation for all tested bituminous binders using developed energy-based crack initiation criterion.

Bitumens	Edge flow damage c_0 (mm)	'Factory-roof' crack a (μm)	Cycles to initiation
Unaged 40/60	0.47	0.46	839
RTFO 40/60	0.68	0.48	1509
PAV 40/60	0.83	0.34	1062
Unaged X-70	0.32	0.45	1750
RTFO X-70	0.55	0.55	2003
PAV X-70	0.68	0.45	4314
PAV base X-70	0.59	0.49	1713
PAV 100/150	0.59	0.51	1791

5.5 Potential application of crack initiation criterion

This energy-based criterion can be potentially applied to determine the critical shear stress for the crack initiation of bituminous binders subjected to the rotational shear fatigue loads. Based on **Eqs. (6)** and **(7)**, *RPSE*(*r*) at the crack initiation position $\left(r_0 - c_0\right)$ is written as

$$RPSE = \frac{1}{2}\frac{\tau_c^2}{G_R} \quad (22)$$

where τ_c is the critical shear stress.

Substituting **Eq. (22)** into **Eq. (16)** and then considering $r_0 - c_0 - a \approx r_0 - c_0$ ($a << c_0$), the critical shear stress can be obtained as

$$\tau_c = 2\sqrt{\frac{\Gamma G_R}{\pi a}} \quad (23)$$

Eq. (23) shows a direct relation of the critical shear stress τ_c with the surface energy Γ, the shear reference modulus G_R and the critical crack size *a*. It is noted that the form of

Eq. (23) is analogous to the well-known solution for the critical tensile stress of an elastic material shown in **Eq. (24)**.

$$\sigma_c = \sqrt{\frac{G_c E}{\pi a}} \tag{24}$$

where σ_c is the critical tensile stress, a is the critical crack size, E is elastic modulus, and G_c is the energy release ratio (surface energy of the crack for brittle materials). Similarly, the critical shear strain can be expressed as

$$\gamma_c = \frac{2}{\left|G_0^*\right|}\sqrt{\frac{\Gamma G_R}{\pi a}} \tag{25}$$

The critical shear stress (**Eq. (23)**) or strain (**Eq. (25)**) identifies the critical condition when the crack initiation occurs in the bituminous binders subjected to the rotational shear fatigue loads. The critical condition for crack initiation is called the endurance limit, which is the maximum amplitude of a cyclic load applied to a material that does not lead to fatigue failure of the material. The critical condition, or endurance limit, for bituminous binders can be measured by a linear amplitude sweep (LAS) test, which is an accelerated bituminous binder fatigue test consisting of a series of cyclic loads with systematically linearly increasing loading amplitudes at a constant frequency. Following the theoretical modelling of crack initiation in this study, the future research will be focused on further validation and engineering application of the fatigue crack initiation criterion in predicting the endurance limit of bituminous binders using the LAS test.

6. Conclusions

In this study, an energy-based crack initiation criterion is developed for the bituminous binders subjected to a rotational shear fatigue load based on mechanics principles and physical facts during the crack initiation process. Laboratory tests including contact angle measurements and DSR tests are conducted to determine the model parameters.

The crack initiation criterion is validated through comparing the predicted and measured surface energy of the bitumen. The major contributions of this study are summarised as follows:

(1) Bitumen fatigue cracking under a rotational shear fatigue load can be divided into two stages: the edge flow damage and the 'factory-roof' cracking.
(2) The edge flow damage can be regarded as a process including the molecular rearrangements, microcrack nucleation and circumferential crack formation.
(3) The local energy redistribution due to the circumferential 'factory-roof' crack is quantified by the pseudostrain energy. A crack initiation criterion is developed for bitumen under a rotational shear fatigue load based on viscoelastic Griffith's fracture mechanics.
(4) The crack initiation is dependent of the shear modulus and surface energy of bituminous binders, critical crack size, and loading amplitude.
(5) The energy-based crack initiation criterion along with the DSR fatigue tests can be used to determine the surface energy of bituminous binders.
(6) The polymer modification can improve the binder resistance to the crack initiation and extend the fatigue crack initiation life.

Acknowledgements

The authors would like to acknowledge the financial support provided by European Union's Horizon 2020 programme via a Marie S. Curie Individual Fellowship project (Grant No. 789551).

References

[1] K.A. Ghuzlan, S.H. Carpenter, Energy-derived, damage-based failure criterion for fatigue testing, Transportation research record, 1723 (2000) 141-149.
[2] D.A. Anderson, Y.M. Le Hir, M.O. Marasteanu, J.-P. Planche, D. Martin, G. Gauthier, Evaluation of fatigue criteria for asphalt binders, Transportation Research Record, 1766 (2001) 48-56.
[3] K.S. Bonnetti, K. Nam, H.U. Bahia, Measuring and defining fatigue behavior of asphalt binders, Transportation Research Record, 1810 (2002) 33-43.
[4] S. Shen, S.H. Carpenter, Application of the dissipated energy concept in fatigue endurance

limit testing, Transportation Research Record, 1929 (2005) 165-173.
[5] S. Shen, G.D. Airey, S.H. Carpenter, H. Huang, A dissipated energy approach to fatigue evaluation, Road Materials and Pavement Design, 7 (2006) 47-69.
[6] S. Shen, H.-M. Chiu, H. Huang, Characterization of fatigue and healing in asphalt binders, Journal of Materials in Civil Engineering, 22 (2010) 846-852.
[7] A. Akbari, A. Modarres, Evaluating the effect of nano-clay and nano-alumina on the fatigue response of bitumen using strain and time sweep tests, International Journal of Fatigue, 114 (2018) 311-322.
[8] C. Hintz, R. Velasquez, C. Johnson, H. Bahia, Modification and validation of linear amplitude sweep test for binder fatigue specification, Transportation Research Record, 2207 (2011) 99-106.
[9] C. Hintz, H. Bahia, Simplification of linear amplitude sweep test and specification parameter, Transportation Research Record, 2370 (2013) 10-16.
[10] J.Y.M. Nuñez, E.D. Leonel, A.L. Faxina, Fatigue characteristics of modified asphalt binders using fracture mechanics, Engineering Fracture Mechanics, 154 (2016) 1-11.
[11] W. Cao, C. Wang, Fatigue performance characterization and prediction of asphalt binders using the linear amplitude sweep based viscoelastic continuum damage approach, International Journal of Fatigue, 119 (2019) 112-125.
[12] B.S. Underwood, A continuum damage model for asphalt cement and asphalt mastic fatigue, International Journal of Fatigue, 82 (2016) 387-401.
[13] Y. Zhang, Y. Gao, Predicting crack growth in viscoelastic bitumen under a rotational shear fatigue load, Road Materials and Pavement Design, (2019) 1-20.
[14] C. Hintz, H. Bahia, Understanding mechanisms leading to asphalt binder fatigue in the dynamic shear rheometer, Road Materials and Pavement Design, 14 (2013) 231-251.
[15] Y. Gao, L. Li, Y. Zhang, Modeling Crack Propagation in Bituminous Binders under a Rotational Shear Fatigue Load using Pseudo J-Integral Paris' Law, Transportation Research Record, (2020) 0361198119899151.
[16] Y. Zhang, R. Luo, R.L. Lytton, Anisotropic characterization of crack growth in the tertiary flow of asphalt mixtures in compression, Journal of Engineering Mechanics, 140 (2013) 04014032.
[17] Y. Zhang, F. Gu, B. Birgisson, R.L. Lytton, Modelling cracking damage of asphalt mixtures under compressive monotonic and repeated loads using pseudo J-integral Paris' law, Road Materials and Pavement Design, 19 (2018) 525-535.
[18] L. Brown, Dislocation substructures and the initiation of cracks by fatigue, Metal Science, 11 (1977) 315-320.
[19] K.S. Chan, A microstructure-based fatigue-crack-initiation model, Metallurgical and

Materials Transactions A, 34 (2003) 43-58.

[20] K. Tanaka, T. Mura, A dislocation model for fatigue crack initiation, Journal of Applied Mechanics, 48 (1981) 97-103.

[21] G. Venkataraman, Y.-W. Chung, T. Mura, Application of minimum energy formalism in a multiple slip band model for fatigue—I. Calculation of slip band spacings, Acta Metallurgica et Materialia, 39 (1991) 2621-2629.

[22] W. Bascom, R. Cottington, R. Jones, P. Peyser, The fracture of epoxy-and elastomer-modified epoxy polymers in bulk and as adhesives, Journal of Applied Polymer Science, 19 (1975) 2545-2562.

[23] Y.-W. Mai, B. Cotterell, On the essential work of ductile fracture in polymers, International Journal of Fracture, 32 (1986) 105-125.

[24] H. Brown, I. Ward, Craze shape and fracture in poly (methyl methacrylate), Polymer, 14 (1973) 469-475.

[25] C. Hui, A. Ruina, C. Creton, E. Kramer, Micromechanics of crack growth into a craze in a polymer glass, Macromolecules, 25 (1992) 3948-3955.

[26] R.P. Kambour, Mechanism of fracture in glassy polymers. III. Direct observation of the craze ahead of the propagating crack in poly (methyl methacrylate) and polystyrene, Journal of Polymer Science Part A-2: Polymer Physics, 4 (1966) 349-358.

[27] W. Knauss, Stable and unstable crack growth in viscoelastic media, Transactions of the Society of Rheology, 13 (1969) 291-313.

[28] R.A. Schapery, A theory of crack initiation and growth in viscoelastic media, International Journal of Fracture, 11 (1975) 141-159.

[29] A.A. Griffith, VI. The phenomena of rupture and flow in solids, Philosophical transactions of the royal society of london. Series A, containing papers of a mathematical or physical character, 221 (1921) 163-198.

[30] R. Christensen, A rate-dependent criterion for crack growth, International Journal of Fracture, 15 (1979) 3-21.

[31] R.Y. Liang, J. Zhou, Energy based approach for crack initiation and propagation in viscoelastic solid, Engineering Fracture Mechanics, 58 (1997) 71-85.

[32] L. Nikitin, Application of the Griffith's approach to analysis of rupture in viscoelastic bodies, International Journal of Fracture, 24 (1984) 149-157.

[33] F. Dubois, C. Petit, Modelling of the crack growth initiation in viscoelastic media by the $G\theta v$-integral, Engineering Fracture Mechanics, 72 (2005) 2821-2836.

[34] X. Luo, R. Luo, R.L. Lytton, Energy-based crack initiation criterion for viscoelastoplastic materials with distributed cracks, Journal of Engineering Mechanics, 141 (2014) 04014114.

[35] Y. Zhang, X. Luo, R. Luo, R.L. Lytton, Crack initiation in asphalt mixtures under external

compressive loads, Construction and Building Materials, 72 (2014) 94-103.

[36] R.L. Lytton, Y. Zhang, F. Gu, X. Luo, Characteristics of damaged asphalt mixtures in tension and compression, International Journal of Pavement Engineering, 19 (2018) 292-306.

[37] ASTM, Standard test method for effect of heat and air on a moving film of asphalt (rolling thin-film oven test), in, ASTM International, United States 2012.

[38] ASTM, Standard practice for accelerated aging of asphalt binder using a pressurized aging vessel (PAV), in, ASTM International, United States 2013.

[39] Y. Tan, M. Guo, Using surface free energy method to study the cohesion and adhesion of asphalt mastic, Construction and Building Materials, 47 (2013) 254-260.

[40] M. Koc, R. Bulut, Assessment of a sessile drop device and a new testing approach measuring contact angles on aggregates and asphalt binders, Journal of Materials in Civil Engineering, 26 (2013) 391-398.

[41] R. Moraes, R. Velasquez, H. Bahia, Using bond strength and surface energy to estimate moisture resistance of asphalt-aggregate systems, Construction and Building Materials, 130 (2017) 156-170.

[42] C.J. van Oss, M. Chaudhury, R.J. Good, Monopolar surfaces, Advances in colloid and interface science, 28 (1987) 35-64.

[43] C. Wang, H. Zhang, C. Castorena, J. Zhang, Y.R. Kim, Identifying fatigue failure in asphalt binder time sweep tests, Construction and Building Materials, 121 (2016) 535-546.

[44] R.A. Schapery, Correspondence principles and a generalizedJ integral for large deformation and fracture analysis of viscoelastic media, International Journal of Fracture, 25 (1984) 195-223.

[45] Y. Zhang, R. Luo, R.L. Lytton, Characterizing permanent deformation and fracture of asphalt mixtures by using compressive dynamic modulus tests, Journal of Materials in Civil Engineering, 24 (2011) 898-906.

[46] Y. Zhang, R. Luo, R.L. Lytton, Mechanistic modeling of fracture in asphalt mixtures under compressive loading, Journal of Materials in Civil Engineering, 25 (2012) 1189-1197.

[47] Y. Zhang, X. Luo, Y. Deng, S. Hou, X. Shi, R.L. Lytton, Evaluation of rutting potential of flexible pavement structures using energy-based pseudo variables, Construction and Building Materials, 247 (2020) 118391.

[48] A. Schmets, N. Kringos, A. Scarpas, C. Duif, G. Schitter, T. Pauli, First-principles investigation of the multiple phases in bituminous materials: the case of asphaltene stacking, Advanced Testing and Characterisation of Bituminous Materials, 1 (2009) 143-150.

[49] R. Jahangir, D. Little, A. Bhasin, Evolution of asphalt binder microstructure due to tensile loading determined using AFM and image analysis techniques, International Journal of

Pavement Engineering, 16 (2015) 337-349.

[50] L. Shan, Y. Tan, S. Underwood, Y.R. Kim, Application of thixotropy to analyze fatigue and healing characteristics of asphalt binder, Transportation Research Record, 2179 (2010) 85-92.

[51] R. Doremus, Cracks and energy—Criteria for brittle fracture, Journal of Applied Physics, 47 (1976) 1833-1836.

[52] A. Gent, O. Yeoh, Crack growth in twisted rubber disks. Part 3. Effects of crack depth and location, Rubber Chemistry and Technology, 76 (2003) 1276-1289.

[53] C.J. Van Oss, M.K. Chaudhury, R.J. Good, Interfacial Lifshitz-van der Waals and polar interactions in macroscopic systems, Chemical Reviews, 88 (1988) 927-941.

[54] C.J. van Oss, Use of the combined Lifshitz–van der Waals and Lewis acid–base approaches in determining the apolar and polar contributions to surface and interfacial tensions and free energies, Journal of Adhesion Science and Technology, 16 (2002) 669-677.

[55] H.-J. Lee, Y.R. Kim, Viscoelastic constitutive model for asphalt concrete under cyclic loading, Journal of Engineering Mechanics, 124 (1998) 32-40.

[56] N.H. Gibson, C.W. Schwartz, R.A. Schapery, M.W. Witczak, Viscoelastic, viscoplastic, and damage modeling of asphalt concrete in unconfined compression, Transportation Research Record, 1860 (2003) 3-15.